This is a repository copy of *Mapping VIS-terahertz (≤17 THz) surface plasmons sustained on native and chemically functionalized percolated gold thin films using EELS.*.

White Rose Research Online URL for this paper:
https://eprints.whiterose.ac.uk/125291/

Version: Accepted Version

Mapping electric fields in the VIS-terahertz (≤ 17 THz) spectral range localized on native and chemically functionalized percolated gold thin films using EELS

Patricia Abellan[1] Patrick Z. El-Khoury[2] and Quentin M. Ramasse[1]*

[1]SuperSTEM Laboratory, SciTech Daresbury Campus, Keckwick Lane, Daresbury WA4 4AD, U.K.

[2]Physical and Computational Sciences Directorate, Pacific Northwest National Laboratory, Richland, WA 99352, U.S.A.

[*]Corresponding author: pabellan@superstem.org

ABSTRACT

Heterogeneous assemblies of molecules (Rhodamine B) adsorbed onto a nano-corrugated metallic surface (a percolated Au network) are investigated using electron energy loss spectroscopy in the scanning transmission electron microscope (STEM-EELS). Our first measurements target the native metallic substrate, which consists of a commercial Au thin film atop an ultrathin carbon membrane. The Au film displays a percolated morphology with nanostructures of estimated thickness $\leq$ 10nm approximately. We observe a rich plasmonic response from the metallic substrate; one which varies nanometrically and spans the VIS-terahertz region. Multiple localized fields are detected at individual nanometric integrated areas, while an analysis of their spatial distribution reveal that for each integrated energy range (50meV integration window) resonances are simultaneously supported at different locations within the film. We record subsequent EEL spectrum images of the hybrid molecular-metallic construct after deposition of Rhodamine B molecules onto the substrate, where plasmons, molecular vibrations and electronic excitations might all be simultaneously detected. A comparison of average signals for both systems is performed and spectral variations within the three spectral regions where molecular signatures may be observed are discussed. Our measurements and their analysis, if applied to the same location before and after molecular deposition, may be used to rationalize optical microscopic and spectroscopic measurements that take advantage of the interplay between molecules and plasmons.

Introduction

Hybrid molecular-metallic constructs have found applications in fields as diverse as photo-catalysis, chemical/biological/medical detection and imaging, as well as photovoltaics, to name a few.[1-4] Beyond a handful of proof-of-principle demonstrations, where precise nano-architectures are constructed and addressed in correlated microscopic and/or spectroscopic measurements, heterogeneity (spatial and hence spectral) in both the molecular and metallic domains is the rule rather than the exception. In the field of plasmon-enhanced optical microscopy and spectroscopy, heterogeneous metallic surfaces (electrodes) rather than precisely controlled nanostructured templates were behind the first observations of surface-enhanced Raman scattering (SERS). Roughened metallic surfaces are thought to sustain a rich variety of plasmonic properties, which can complicate the interpretation of optical signals emanating from metals or the typically ill-defined distributions of molecules in their immediate vicinity,[5] as well as molecule-metal interactions.[6, 7] Although optical approaches may effectively be used to fingerprint single molecules, e.g. *via* SERS,[2, 8] it has been indeed recognized that signals collected from a relative large diffraction-limited area are dominated by the response of a few molecules located at plasmonic hot-spots[9] (specific sites on the plasmonic substrate that are optimally excited with the incident laser beam used for Raman microscopy and spectroscopy). In random metallic thin films, the resulting hot-spots can produce especially large enhancement factors, which have been used for single molecule detection in a number of works.[10, 11] The limited spatial resolution available in optical measurements when resolving the structural details of samples coupled with the limited spectral range (e.g. a finite set of laser lines used in any particular optical

measurement) together necessitate a different approach to characterizing more precisely molecular distributions near roughened metals (*i.e.* realistic constructs).

Beyond the near-UV-Visible-near-IR spectral region, where most plasmon-enhanced optical spectroscopies based on silver and gold nanostructures are focused, recent advances in nanophotonics[12] motivate the identification and characterization of novel constructs that support local electric fields in the teraherz regime.[13] Infrared plasmons are encountered in semiconducting materials with plasma energies that can be tuned by doping,[14] and in low-dimensional materials like graphene,[15] where the plasmon can be also tuned to mid-infrared and terahertz. Other approaches are based on the creation of a linear array of subwavelength grooves supporting tightly confined *spoof* plasmons[16] or on the design of plasmonic meta-surfaces for subwavelength guiding of THz surface waves.[17] One of the main motivations behind terahertz plasmonics and terahertz local fields has to do with the fact that non-ionizing radiation in this regime can travel through opaque materials with minimal damage, which is ideal for biological and biomedical applications. Also, it has been recently demonstrated that when there is a spectral overlap between the molecules absorbance and the localized surface plasmon resonances (LSPRs), plasmonic-molecular resonance coupling may occur,[18, 19] ultimately enabling LSPR-based small molecule detection. The latter is due to the fact that the effectiveness of plasmonic nanosensors for detecting the refractive index of analytes will depend of their molecular weight.[20] Nonetheless, despite these promising properties, terahertz local fields are somewhat elusive, in part because of the challenges involved in characterizing constructs in this spectral range with the relevant nanometer spatial resolution.

Electron energy loss spectroscopy (EELS) allows us to investigate the plasmonic fields of metal nanostructures in a broad range of energies and to perform a direct correlation with atomic scale

images of the area. By combining electron source monochromation and iterative Richardson-Lucy deconvolution, the detection of localized surface Plasmon resonances (LSPRs) at energies as low as 330meV has been demonstrated in studies of the optical response of silver squares (up to 1µm in size).[21] These numerical deconvolution methods require large signal-to-noise ratios in the raw data to avoid numerical processing artefacts; these are rarely achievable when working with beam sensitive materials, such as in molecules-containing systems, thus precluding in most cases the application of deconvolution algorithms in metal-molecular constructs. Making use of a new monochromator design which provides incident beam energies down to the 10meV range[22] (to optimize signal-to-noise, the beam energy as evaluated from the zero-loss-peak full-width at half-maximum in this work was 22meV), directly detecting plasmons and mapping the resulting fields down to the mid-IR and THz regime is in principle possible. Besides the plasmonic signals, EELS can simultaneously detect vibrational states of the molecules which also lie in the THz spectral region (<110 THz). Altogether this provides a unique opportunity not only to characterize a substrate sustaining THz Plasmons but also the effect of plasmonic fields lying within the energy values of the vibrational states of molecules.

Here we measure nanometrically varying surface plasmon modes and local electric fields on a commercial Au plasmonic substrate providing a quasi-continuous generation of enhanced fields covering the <70meV-2.5eV energy range. We investigate a common configuration used for molecular sensing consisting of random arrangements of Au elongated networks on a thin carbon film. We then drop cast a solution of Rhodamine B molecules, which forms droplets of about 50-250nm in diameter. We observe rapid spatial changes, at the nm scale, of the resonant signals and compare normalized signals recorded from relatively large (fields-of-view up to 150nm x

150nm) areas between the Au templates with Rhodamine B and the plain templates to examine any evidence of interplay between the molecules and the plasmonic metal in our construct.

Results

Figure 1(a) shows a high-angle annular dark field (HAADF, often referred to as Z-contrast due to the intensity's $\sim Z^{1.7}$ dependence on the atomic number Z of the object) image of a commercial substrate consisting of a thin Au deposit on a carbon membrane, with a nominal effective thickness of 2-3nm, displaying de-wetting to a final percolated Au film morphology of nominal feature size of 5±1 nm (Substratek™, Ted Pella, Inc). Samples were heated to a steady temperature of 65°C for 24 hours prior to their investigation by EELS to minimize hydrocarbon-based contamination build-up. The experimentally-estimated thickness of the observed films by EELS (see methods section for details) was ~11nm for the underlying carbon films, whereas the Au nanostructures were ≤ 10 nm in thickness in the areas observed in this work. While this measure value is slightly higher than the quoted nominal thickness of the film, the discrepancy could simply be due to natural variability across the grid (only a relatively small portion of which was observed), in addition to the intrinsic uncertainty in the EELS thickness measurement. The mild heating treatment described above is unlikely to have resulted in any significant coarsening of the Au nanostructure, however. Figure 1 (b) shows averaged, background-subtracted (using a simple power-law function model) EEL spectra selected from a spectrum image consisting on 100x100 individual spectra collected over the field of view of 800nm in lateral size shown in (a). The signals in (b) are the result of averaging 4 individual spectra over the 16nmx16nm areas indicated with numbers 1 through 18 in (a) and normalized by the total number of counts in the

corresponding raw spectra for each region. Due to the intrinsic noisy nature of the signal in this energy range, a gentle smoothing was applied to the spectra (Savitzky-Golay filter overlaid on top of the unprocessed data in lighter colors). A large number of localized electric fields were resolved for energies below the main surface plasmon resonance (LSPR) of Au (at about 2.1eV in average) down to well below 70meV, *vide infra*. For each integrated area (with 16nm x 16nm dimensions in this case), different plasmon resonances are simultaneously detected with energies spanning over the whole detection range described above. The spatial distributions of some of these resonances, for different energy ranges indicated in the images and with a spectral integration width of 50meV (12 THz approx.), are shown in Figure 1 (c). Overall, the spatial distribution of the localized fields appears random; with fields contained within the integrated energy ranges *lighting up* at different locations within our 800nm field of view for each energy window mapped. To illustrate this disparity in the distribution of local fields, an average of the 100x100 spectra in the spectrum image acquired in the region in (a) is shown in (d). The spectrum shows the measured energy loss signal in the entire energy range with a broad peak with maximum signal around the surface plasmon resonance of Au (~2.1eV) and increasing signals at lower energies. The range of plasmonic signals localized within the percolated Au network may expand over a broader energy range including many lower energy features for which resonances would be hidden within the tail of the zero-loss peak (ZLP).

Figure 2 shows the raw spectrum and background-subtracted signal for region 1 in Figure 1. As indicated by an arrow, a well-resolved resonance at 70meV (17 THz) is directly detected in the averaged spectrum. In order to provide an acceptable compromise between signal-to-noise and acquisition time (with the experiments involving molecular deposits in mind, in particular), the beam monochromator was adjusted to a ~22meV resolution, as measured by the full-width at

half-maximum (FWHM) of the ZLP through the carbon membrane (the effective resolution, in vacuum, would have been below this value, likely ~18meV). Although a higher energy resolution (resolutions of 12-14meV have been demonstrated on this instrument)[6, 23] would most likely enable the observation of lower energy local electric fields, our measurements represent a direct detection of a broad range of frequencies from ≤17 THz to up to 532THz (0.07-2.2 eV).

Rhodamine B molecules were deposited on fresh substrates from the same commercial batch (and therefore assumed to be entirely comparable) and submitted to the same heating procedure prior to their observation by STEM-EELS. Figure 3 (a)-(c) show HAADF (a) and medium angle annular dark field (MAADF), (b) and (c), images of 100-250nm droplets of Rhodamine B formed upon drop-casting of a 1mM solution of Rhodamine B in methanol dried on the surface of the Au nanostructured film. The contours of the circular molecular deposits were more readily visible using the narrower angular detector range of the MAADF images as compared to the pure Z-contrast of HAADF images. From our intensity profiles (not shown), this could be due to both: higher relative intensity of the molecular deposits in the MAADF images together with lower contrast observed between the intensity arising from the Au film and from the C substrate (for the overlaid molecular layer the latter translates into a lower contrast background). We note that the nonlinearity in the signal scaling with atomic number for MAADF images and an increase in signal intensity compared to Z-contrast images have both been demonstrated for single and double layers of graphene and boron nitride.[24] The image in (d) is a HAADF image taken simultaneously with a spectrum image comprising 80 x 80 pixels over a 150nm field-of-view. The spectra shown immediately underneath this 'survey' image were extracted and averaged from the areas indicated by labels 1-10 in the image and with dimensions 9.4 nm x 9.4 nm. The signals shown are averaged over 5x5 EELS spectra and normalized to the total counts of the raw

EELS data in each integrated area. As shown in the spectra, the signals of the plasmon resonances are strongly damped once the molecules cover the surface: indeed, assuming the substrates are entirely comparable between the two experiments (with and without molecular deposits), the same rich and varied distribution of THz-level resonances would have been expected here. Instead, a modulation of the spectra is evident with individual resonances appearing broader than in the plain substrate in Figure 1 (b). Importantly, two peaks, consistent with the two broad vibrational bands for Rhodamine B as measured by EELS[25] are observed in all spectra. Namely, a large vibrational band between 100-200 meV and a second band in the 350-450meV energy region are detected. The energy region located between the two vibrational bands, which typically should not show any vibrational signal, as well as the signal across the vibrational bands themselves, present large variability.

In order to identify general spectral features characteristic of the plain ultra-thin Au (denoted UTAu thereafter) and of UTAu films with molecules, average normalized spectra collected from relatively broad square areas (of 150 nm lateral size approx.) were compared, see Figure 4(a). As already mentioned for the average spectrum from the UTAu film in Figure 1 (d), both average spectra in Figure 4 display broad resonances with a maximum energy value lying around the main surface-plasmon energy of gold. For the sample with Rhodamine B molecules (RhB) at the surface (denoted RhB:UTAu thereafter), the increase in overall sample thickness due to the presence of the molecular deposit, results in largersignals arising from higher energy inelastic scattering and interband transitions (broad distribution peaked at a higher energy, not within the displayed energy window but whose increase is clearly seen here for $\geq 2.5eV$). A main difference within the 100-200meV energy range is a clear increase in the energy loss for the case of RhB:UTAu sample. This was expected, as most vibrational states for RhB fall within this

energy range. Interestingly, the plain UTAu substrates still display a clear feature at these same energies. The narrower shoulder around the 350-450meV energy range registered only for the RhB:UTAu samples correspond to a second set of vibrational states of the molecules. A relative decrease in the energy loss within 0.5-1.5eV for the RhB:UTAu sample (as compared to the plain gold substrate) can be explained by the damping of the LSPRs due to the increase in refractive index at the metal surface by the molecular layer. We note that if the energy loss didn't increase due to thickness effects mentioned above, this relative decrease of all signals arise from the local electric fields would also undergo for the 1.5-2.5eV energies.

Figures 4 (b) - (d) show vibrational bands, (b) and (c) averaged over a 90nmx95nm region, as well as the main surface plasmon of Au, (d) averaged over 78nm x 170nm. The spectra were background-subtracted using a power-law model – in order to better isolate the various spectral contributions from the ZLP tail. Blue dots and red squares overlaid the spectra in (b) and (c) indicate the energy positions of experimentally detected IR-active and Raman-active main resonances, respectively.[25] As shown in (b), the fine structure superposed on the broadband signal is consistent with main optical resonances. Additional features are also observed that cannot be assigned at present. The blue arrows in the spectra indicate the strongest IR-active mode for Rhodamine B within the two vibrational bands. For the lowest vibrational band in (b), this value together with the superimposed Raman-active and IR-active modes at a slightly higher energy is consistent with the maximum number of counts measured by EELS. For the higher vibrational band in (c), we note that Rhodamine B only has IR-active modes and its strongest mode corresponds to the maximum value for EELS as well. Interestingly, as compared to measurements of the same molecule in carbon and silicon substrates,[25] the fine structure, and most importantly the maxima positions for both bands, in the present measurements appears

somehow better defined on this substrate. This is, however, a preliminary observation that would require future confirmation. In addition, the average EELS signal was also isolated following a similar procedure for the case of the 1.2-3.2eV energy range, where both the surface Plasmon of Au and the excited electronic states of Rhodamine B lie (two emission peaks within 2.1-2.3eV energy range)[26].

Figure 4 (d) compares this energy region for a bare UTAu sample and for the RhB molecules on the UTAu surface. Besides a broad plasmon resonance centered at about 2.1eV, corresponding to the main surface plasmon of Au, another plasmon resonance is observed in both sets of measurements, indicated by arrows in Figure 4(d). As data was collected during different microscope sessions and is displayed without any processing, we thus identify these features as intrinsic (plasmonic features) to the UTAu substrate (see the experimental section for details on gain correction and correlated noise minimization). We note that, on average, the deposition of molecules does not result in any observable shift of the main surface plasmon maximum, even though the spectra from smaller integrated areas presents some variability. To illustrate this, Figure 4 (e) show plasmon peak maps for energy loss integration windows 1.91-2.01eV and for 2.13-2.23eV. The spectra in (e) are plotted using the same intensity scale and have not been normalized to account for inhomogenieties on the molecular coverage due to high nose levels on thicker areas. Despite this fact, the maps show enlarge signals along the particle surface with local maxima that varies for different locations and energy ranges. Two arrows on the bottom spectrum indicate additional features observed only in the average spectrum from the molecular deposited-sample. The spectrum of the RhB:UTAu sample is nosier than that of the bare percolated film, as the exposure time was kept short to minimize any damage to the molecules. Assigning these two features as meaningful signal is thus not completely

unambiguous, but they do lie at energy values for which excited electronic states of Rhodamine B on carbon substrates have been measured[25] and the observed peaks are marginally above the noise level (on-par with the plasmonic feature identified at 1.7eV, for instance).

Vibrational signals and low loss energy signals in EEL experiments can arise from a number of sources. Relativistic effects such as Čerenkov and guided light modes[27-29] in particular are always a concern as they can make the interpretation of the low loss signal challenging if not properly considered. Due to the metallic nature of the samples, we do not expect Čerenkov radiation influencing the present measurements. Nevertheless, we note for completeness that the critical refractive index for Čerenkov emission for an incident electron energy of 60kV would be roughly n=2.[30] While the refractive index for Au is very low for higher energies (0.92 for 1.937μm corresponding to 640meV)[31], it increases in the THz regimes and for 60THz its experimental values is above the critical value for Čerenkov emission (n between 2.5 and 3 measured for a 75nm thin Au film)[32]. For the case of carbon, the refractive index for 70meV is around n=3.0.[33] Regarding vibrational signals arising from sources other than the Rhodamine B molecules of interest, we note first that an advantage of the application of metallic templates to the study of the molecules and of any possible effect from metal-molecules interactions is that it avoids the use of nanoparticles, which often include capping agents that will impact the measured EELS signal if the capping agent is not carefully removed.[25] On the other hand, amorphous carbon from the support might contribute to the overall vibrational signal detected with a broad peak within the wavelength range of 1200 – 1600 cm^{-1} (roughly 136-200eV).[34] In other EELS work, a broad excitation centered at approximately 150meV was attributed to the contribution of both the excited modes of amorphous carbon and the coating layer of a MgO nanostructure.[35] Although the latter is a contribution that is most likely present here, and might

indeed contribute to the signal peaking up at around 155meV in the average spectrum for the plain UTAu substrate in Figure 4(a), it is unlikely to mask or influence the narrow low-energy signals changing for each integration area in Figure 1(b). We note also the large differences in the spectra in Figure 3 (d) for the samples with molecules deposited as compare to the plain substrate: clearly, the vibrational signal from Rhodamine B dominates the low loss here, while a slight modulation that changes from area to area is still observed.

The remarkable optical properties of random thin metallic films, as those investigated here, ultimately displaying hot spots with large enhancement factors for optical spectroscopy and microscopy, are believed to arise from complex hybridization between LSPRs. In order to understand these complex processes different optical techniques have been applied. Using nonlinear excitation spectroscopy of single hot spots, the spectral characteristics of the plasmon modes in silver films with different surface coverages and morphologies were investigated.[36, 37] Plasmon resonances located at the hot spots were observed to change from a single broad peak for low coverages (dispersion of isolated nanoparticles) to narrow multi-peaked resonances in high coverages (network morphology similar to that studied in the present work). In these experiments, [36, 37] performed using silver thin films, a single hot spot would then support multiple narrow plasmons spanning across the investigated energy range (1.3-1.8 eV). As shown in Figure 1, our observations also point to a similar behavior for the case of Au where a number of resonances are detected at each point of the sample. We note that this is still the case in measurements integrated over smaller areas using dispersions of 5meV/channel instead (not shown). Crucially, carrying out these experiments using STEM-EELS means that the data span a much broader energy range and as a result we are able to observe that the substrates support resonances at energies as low as 70THz. In related work, nanostructured Au films with similar

morphologies to our substrates were investigated by aberration-corrected photoemission electron microscopy (PEEM).[38] By changing the excitation energy, LSPRs were mapped in different locations of the substrate. In our experiments and thanks to the broad-band nature of EELS measurements we have map different localized electric fields across the entire energy range, showing resonant signals in different locations of the observation area simultaneously. This capability together with the ability of detecting all possible resonances at each individual spot provides the opportunity of performing correlative analysis of the different resonances across the energy range.[39]

Regarding possible plasmon-molecules interaction and in particular the effect of the molecules on the surface plasmon, it is interesting to observe that no obvious shift in the main plasmon energy is observed between the spatially averaged measurement of the surface plasmon of gold in the plain substrate and that of the substrate with Rhodamine B molecules shown in Figure 4 (d). An initial conclusion would thus be that on average the molecules do not seem to affect the metal, certainly at larger length scales. Spectra integrated over much smaller regions (16nm lateral size in Figure 1 for the plain UTAu films and 7.5nm in Figure 4 (e) for the RhB:UTAu sample) indicate, however, local shifts of the plasmon, an effect that would warrant further investigation on its own. Elucidating a possible effect of the molecules on the plasmons at nanometric locations along the film would thus require a comparison before and after molecular deposition in the same exact location. For the case of the vibrational states of the molecules, we note that additional peaks are observed in the vibrational spectrum in Figure 1(b) which cannot be rigorously assigned to any IR or Raman-active modes. Elucidating these effect would require of a systematic investigation where, ideally, the same area in the substrate would be mapped by STEM-EELS before and after molecular deposition.

Conclusions

Using monochromated EELS we investigate the plasmonic properties of heterogeneous randomly oriented thin Au films, displaying a percolated morphology. Our observations show a complex scenario with localized electric fields detected over a broad range of frequencies from ≤17THz up to 532 THz (0.07-2.2 eV). For each nanometric integrated area, different plasmons are excited over the explored energy range. Also, our maps performed in large (800nm of side) areas demonstrate that different locations simultaneously support plasmons within the same energy range (50eV width was used). Rhodamine B molecules were subsequently deposited and the hybridized molecules-metals samples investigated by EELS. The vibrational spectra of the molecules and damping of the plasmonic modes was observed at each position in the sample. Variability in the spectra and, in particular, in the vibrational bands of the molecule is discussed. A future empirical approach has been devised in order to elucidate the origin of the spectral variations, especially with the goal of investigating possible molecules-plasmon interactions, where a specific area of the substrate would be defined and carefully characterized in the microscope prior to further observation of the exact same location after deposition of the molecular system.

Experimental

The Rhodamine B samples were prepared by drop-casting a solution of Rhodamine B molecules in methanol (1 mM) on the Au substrates (Substratek^{TM}, TedPella). EELS measurements were performed using a Nion UltraSTEM 100MC "Hermes" with Nion Quadrupole-Octupole (QO) aberration corrector and a monochromated electron source. All EEL spectra were acquired at an accelerating voltage of 60kV. Collection and convergence angles for EELS were alpha=31mrad and beta=44mrad. Probe size for those settings at 60kV is close to 0.9A. The energy dispersion and full width at half maximum (FWHM) of the zero loss (ZL) peak for each dataset is specified in the figures captions. All EEL spectrum images (SI) from molecules were acquired using a blank survey image, thus the only exposure was during data acquisition. No subpixel scanning was used.

The spectrometer was equipped with a Gatan Enfinium ERS camera. Dark references were automatically acquired after data collection. Besides acquitting gain references for gain correction, binning (over 130 channels) was used and the spectra were let to shift in energy position during acquisition (for the data in Figure 4(d) for instance a shift above 80meV corresponding to >40 channels was observed). Averaging over a number of spectra (specified for each graph in the figure captions), would thus aid supressing residual correlated noise.[40]

The thickness of the carbon film was estimated by collecting EEL spectra from regions free of Au nanostructures and following the log ration technique.[41] The relative thickness ranged between t = 0.14λ – 0.18λ, where λ is the inelastic mean free path of the electrons in the material. This yields absolute thickness values of 10-11 nm. For of the regions containing the percolated Au nanostructures, no direct measurement of the free-standing Au was possible, thus for the relative thickness values of different Au-C regions, namely 0.31λ-0.42λ, λ would correspond to an effective mean free path of the combined Au-C stack. If the combined sample were entirely

made of Au then this relative thickness would be correspond to a stack 10-12nm thick. In the other extreme, if the percolated film were made of carbon (itself sitting on top of a 10-11nm carbon support, from the layer), then the estimated thickness of the percolated film would be 10-15nm. We note that, due to the large difference in atomic number, λ will be mainly influence by the presence of Au. As a result, and even though both thickness estimates above are overestimating the Au film thickness, these measurements indicate that thickness of Au in this sample would most likely be just $t \leq 10$nm.
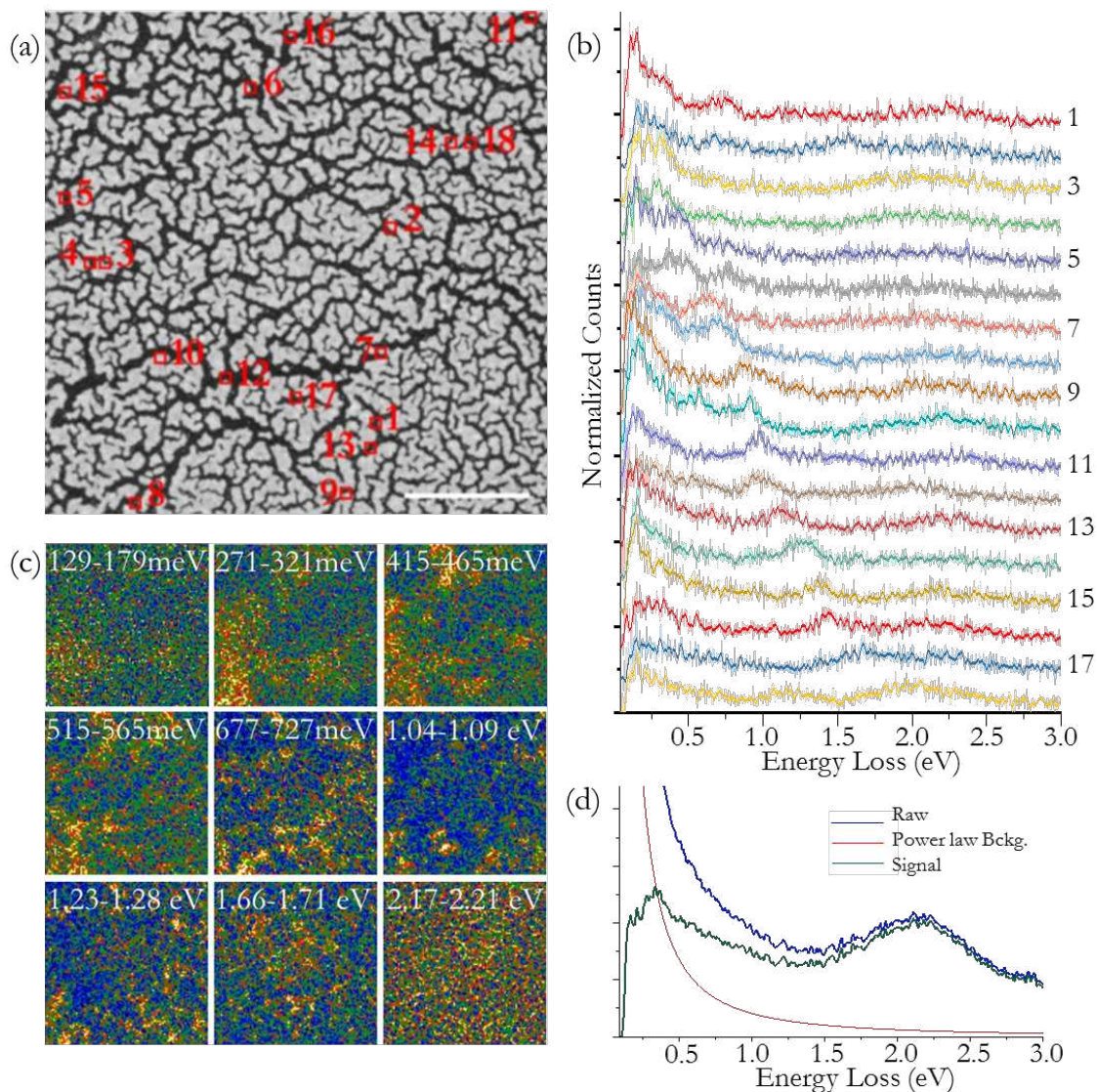
Figure 1: (a) Z-contrast image of the percolated Au film over a field-of-view area of 800nm of size. The scale bar indicates 200nm. This image was used as a spectral image (SI) survey for subsequent EELS SI acquisition. (b) Spectra from areas in (a) indicated as 1 through 18. A Savitzky-Golay filter with 35 points of window and using a 4th order polynomial has been used to smooth the data; thicker lines show the resulting spectra overlaid on top of the unprocessed

data in lighter colors. Raw EELS SI consisted of 100x100 pixels. No subpixel scanning was performed. The integrated areas of the averaged spectra had dimensions of 16nmx16nm, consisting of 2x2 pixels. The dispersion value is 2meV/pixel and the exposure time per spectrum is 28 miliseconds. (c) Integrated signal maps in the energy regions indicated in (a). (d) Spectrum averaged over all the EELS spectra in the spectral image (10000 spectra) before and after power law background subtraction. FWHM of the ZL peak is 22 meV through Au:carbon areas.
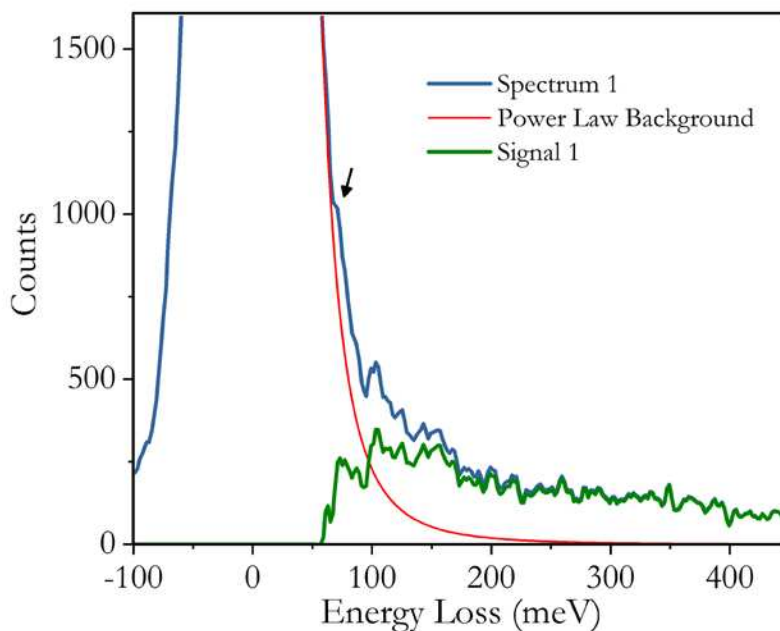

Figure 2: Spectrum in area 1 in Figure 1 displaying plasmonic signals ≤ 70 meV corresponding to 17 THz.
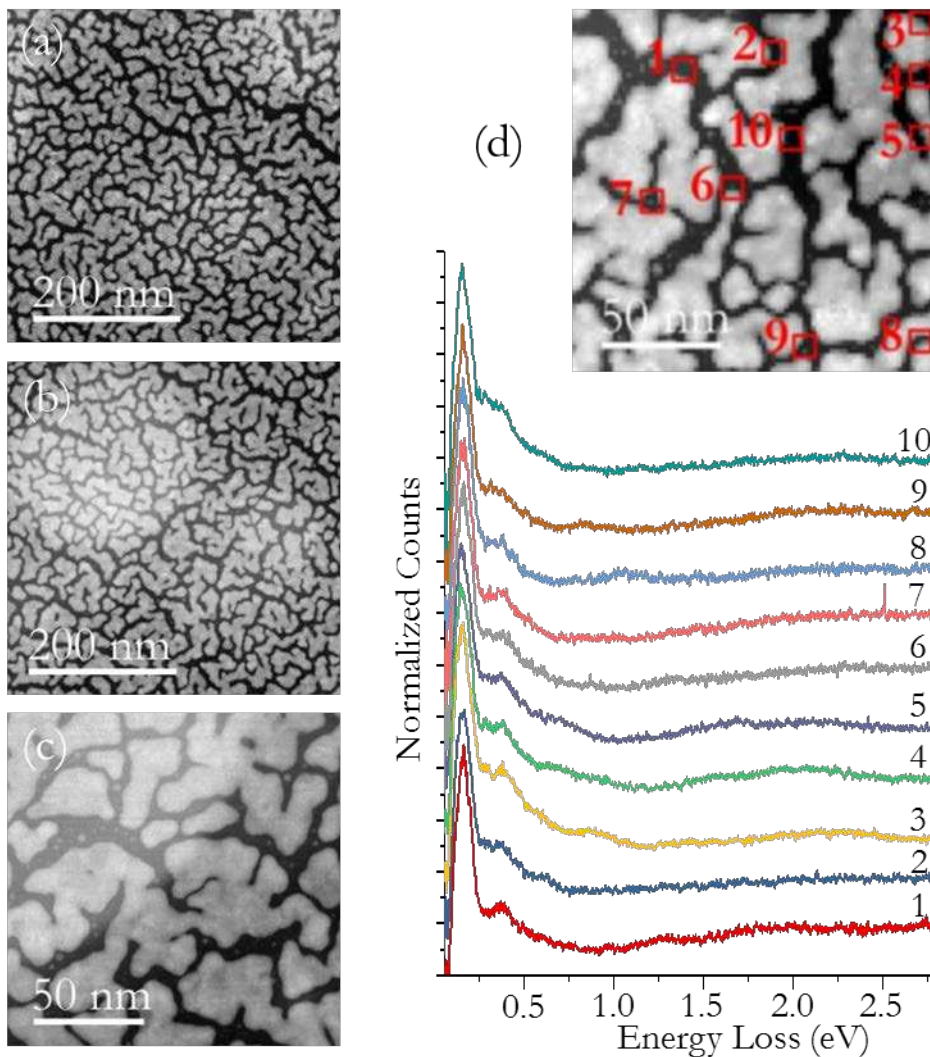
Figure 3: (a) HAADF and (b)-(c) MAADF (middle and bottom) images of nanometric droplets of Rhodamine B molecules. A 1 mM solution of Rhodamine B in methanol was drop casted onto the metallic substrate;drops less than 250nm in diameter are observable. (d) 80 x 80 pixels HAADF image with 1.9nm pixel size recorded simultaneously to a spectral image with the same dimensions. Spectra below are averaged over 5x5 pixels regions of 9.4nm side indicated in the image. The dispersion was set to 2meV/channel at an exposure time of 0.1s with no-subpixel scanning. The area was not exposed to the electron beam prior data collection – the choice of

spectral image was made with the beam blanked and the observation is made through a droplet of molecules. FWHM of the ZL peak is 34 meV through RhB:Au:Carbon areas.
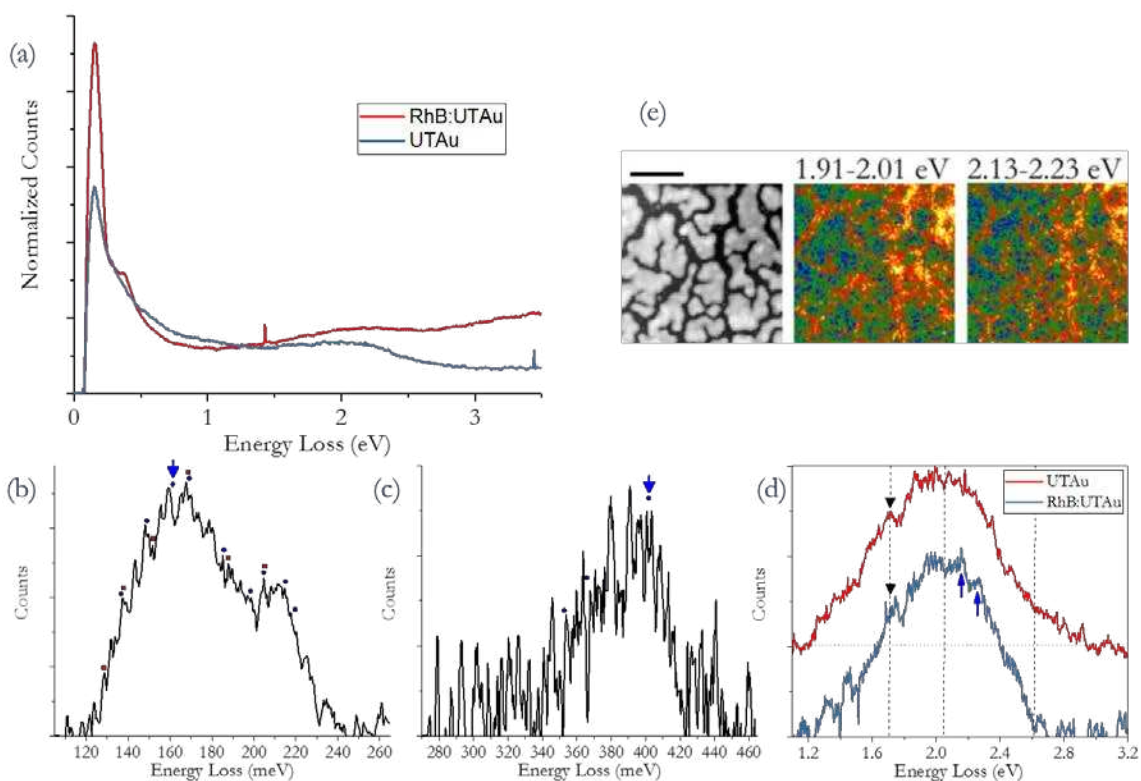

Figure 4: (a) Normalized background subtracted EELS spectra averaged over similar areas of 150 nm x 150 nm (for the RhB:UTAu sample) and 149 nm x 149 nm (UTAu sample). The spectra were normalized to the total counts including the ZLP in the raw average spectra. The dispersion is set to 2meV/channel and no subpixel scanning was used for all acquisitions. For the UTAu sample, the pixel size was 1.7 nm, whereas the FWHM of ZL peak was 34 meV, and the exposure time was 0.058 seconds. For the Rhodamine B-containing sample, the pixel size was 1.9nm, FWHM of ZL peak was 22meV and the exposure time was 0.1 seconds. (b) and (c) Isolated average vibrational bands after background subtraction using two windows and a 2nd

polynomial background fitting. Spectra were averaged over 90nm x 95 nm region (18x19 pixels); exposure time was 0.5 seconds and dispersion 0.5 meV/channel. (d) Isolated surface plasmon using the same background subtraction procedure as for (b) and (c) from an area of 78nmx170nm size using a exposure time of 0.058 seconds (UTAu sample) and 150nmx150nm using exposure time of 0.1 seconds (RhB:UTAu sample). Dispersion was 2meV/channel. (e) Plasmon peak maps for energy ranges indicated (100meV energy window used). Same intensity scale used for both maps. Scale bar on the simultaneously acquired HAADF image was 50nm. Exposure time of 0.1 seconds and dispersion of 2meV/channel was used.

ABBREVIATIONS

STEM, scanning transmission electron microscopy; EELS, electron energy loss spectroscopy; FWHM full width at half maximum; ZLP, zero loss peak; Rhb, Rhodamine B; UTAu, ultra-thin gold; LSP, localized surface plasmon; LSPR, localized surface plasmon resonance.

REFERENCES
1.   E. C. Le Ru and P. G. Etchegoin, *Annual review of physical chemistry*, 2012, 63, 65-87.
2.   S. Nie and S. R. Emory, *science*, 1997, 275, 1102-1106.
3.   R. Zhang, Y. Zhang, Z. Dong, S. Jiang, C. Zhang, L. Chen, L. Zhang, Y. Liao, J. Aizpurua and Y. e. Luo, *Nature*, 2013, 498, 82.
4.   M. L. Brongersma, N. J. Halas and P. Nordlander, *Nat Nano*, 2015, 10, 25-34.

5. P. Z. El-Khoury, G. E. Johnson, I. V. Novikova, Y. Gong, A. G. Joly, J. E. Evans, M. Zamkov, J. Laskin and W. P. Hess, *Faraday discussions*, 2015, 184, 339-357.
6. P. Z. El-Khoury, P. Abellan, Y. Gong, F. Hage, J. Cottom, A. G. Joly, R. Brydson, Q. Ramasse and W. P. Hess, *Analyst*, 2016, 141, 3562-3572.
7. P. Z. El-Khoury, P. Abellan, R. L. Chantry, Y. Gong, A. G. Joly, I. V. Novikova, J. E. Evans, E. Aprà, D. Hu and Q. M. Ramasse, *Advances in Physics: X*, 2016, 1, 35-54.
8. K. Kneipp, Y. Wang, H. Kneipp, L. T. Perelman, I. Itzkan, R. R. Dasari and M. S. Feld, *Physical review letters*, 1997, 78, 1667.
9. Y. Fang, N.-H. Seong and D. D. Dlott, *Science*, 2008, 321, 388.
10. M. J. Walter, J. M. Lupton, K. Becker, J. Feldmann, G. Gaefke and S. Höger, *Physical Review Letters*, 2007, 98, 137401.
11. Y. Saito, J. Wang, D. Batchelder and D. Smith, *Langmuir*, 2003, 19, 6857-6861.
12. E. A. Muller, B. Pollard, H. A. Bechtel, P. van Blerkom and M. B. Raschke, *Science Advances*, 2016, 2.
13. C. T. Cooper, M. Rodriguez, S. Blair and J. S. Shumaker-Parry, *The Journal of Physical Chemistry C*, 2015, 119, 11826-11832.
14. G. Kumar, S. Li, M. M. Jadidi and T. E. Murphy, *New Journal of Physics*, 2013, 15, 085031.
15. F. H. L. Koppens, D. E. Chang and F. J. García de Abajo, *Nano Letters*, 2011, 11, 3370-3377.
16. B. Ng, S. M. Hanham, J. Wu, A. I. Fernández-Domínguez, N. Klein, Y. F. Liew, M. B. H. Breese, M. Hong and S. A. Maier, *ACS Photonics*, 2014, 1, 1059-1067.
17. S. Waselikowski, C. Fischer, J. Wallauer and M. Walther, *New Journal of Physics*, 2013, 15, 075005.
18. L. Guo, J. A. Jackman, H.-H. Yang, P. Chen, N.-J. Cho and D.-H. Kim, *Nano Today*, 2015, 10, 213-239.
19. J. Zhao, L. Jensen, J. Sung, S. Zou, G. C. Schatz and R. P. Van Duyne, *Journal of the American Chemical Society*, 2007, 129, 7647-7656.
20. J. N. Anker, W. P. Hall, O. Lyandres, N. C. Shah, J. Zhao and R. P. Van Duyne, *Nature materials*, 2008, 7, 442-453.
21. E. P. Bellido, A. Manjavacas, Y. Zhang, Y. Cao, P. Nordlander and G. A. Botton, *ACS Photonics*, 2016, 3, 428-433.
22. O. L. Krivanek, T. C. Lovejoy, N. Dellby, T. Aoki, R. W. Carpenter, P. Rez, E. Soignard, J. Zhu, P. E. Batson, M. J. Lagos, R. F. Egerton and P. A. Crozier, *Nature*, 2014, 514, 209-212.
23. P. Abellan, P. Z. El-Khoury, F. S. Hage, J. Cottom, A. G. Joly, W. P. Hess, R. Brydson and Q. M. Ramasse, *Microscopy and Microanalysis*, 2017, 23, 1540-1541.
24. O. L. Krivanek, M. F. Chisholm, V. Nicolosi, T. J. Pennycook, G. J. Corbin, N. Dellby, M. F. Murfitt, C. S. Own, Z. S. Szilagyi, M. P. Oxley, S. T. Pantelides and S. J. Pennycook, *Nature*, 2010, 464, 571-574.
25. P. Abellan, P. Z. El-Khoury, F. S. Hage, W. P. Hess, R. Brydson and Q. M. Ramasse, *Submitted*, 2017.
26. F. Köhn, J. Hofkens and F. De Schryver, *Chemical Physics Letters*, 2000, 321, 372-378.
27. R. Erni and N. D. Browning, *Ultramicroscopy*, 2008, 108, 84-99.
28. M. Stöger-Pollach and P. Schattschneider, *Ultramicroscopy*, 2007, 107, 1178-1185.
29. R. Erni, *Ultramicroscopy*, 2016, 160, 80-83.

30. P. A. Crozier, *Ultramicroscopy*, 2017, 180, 104-114.
31. P. B. Johnson and R.-W. Christy, *Physical review B*, 1972, 6, 4370.
32. M. N. Gadalla, M. Abdel-Rahman and A. Shamim, 2014, 4, 4270.
33. H. J. Hagemann, W. Gudat and C. Kunz, *J. Opt. Soc. Am.*, 1975, 65, 742-744.
34. P. K. Chu and L. Li, *Materials Chemistry and Physics*, 2006, 96, 253-277.
35. M. J. Lagos, A. Trügler, U. Hohenester and P. E. Batson, *Nature*, 2017, 543, 529-532.
36. N. J. Borys and J. M. Lupton, *The Journal of Physical Chemistry C*, 2011, 115, 13645-13659.
37. N. J. Borys, E. Shafran and J. M. Lupton, *Scientific reports*, 2013, 3.
38. R. C. Word, J. Fitzgerald and R. Könenkamp, *Surface Science*, 2013, 607, 148-152.
39. A. Losquin, S. Camelio, D. Rossouw, M. Besbes, F. Pailloux, D. Babonneau, G. A. Botton, J.-J. Greffet, O. Stéphan and M. Kociak, *Physical Review B*, 2013, 88, 115427.
40. M. Bosman and V. J. Keast, *Ultramicroscopy*, 2008, 108, 837-846.
41. R. F. Egerton, *Electron energy-loss spectroscopy in the electron microscope*, Springer Science & Business Media, 2011.